ELSEVIER

Polymer 41 (2000) 5471–5483

polymer

Effect of rubber functionality on microstructures and fracture toughness of impact-modified nylon 6,6/polypropylene blends Part II. Toughening mechanisms

Shing-Chung Wong, Yiu-Wing Mai[1,*]

Center for Advanced Materials Technology (CAMT), Department of Mechanical and Mechatronic Engineering J07, The University of Sydney, Sydney, NSW 2006, Australia

Received 14 December 1998; received in revised form 15 September 1999; accepted 14 October 1999

Abstract

Toughening mechanisms in blends containing 60 parts nylon 6,6, 20 parts polypropylene (PP) and 20 parts styrene–ethylene/butylene–styrene (SEBS) grafted to different levels of maleic anhydride (MA) were investigated. The sequence of events was carefully characterised using different microscopic techniques. It was found that under triaxial constraint interfacial cavitation followed by multiple crazing and subsequently massive shear yielding of the matrix contributed to an enormous toughening effect in core-shell microstructures observed in 0.92%-maleated blend (0.74% in Part I paper [Wong SC, Mai Y-W. Polymer, 1999;40:1553], should be 0.92% as corrected in this paper). The core-shell structure was formed when the spherical domains of PP were surrounded by SEBS rubber in a nylon-rich matrix.. In this composition, miscibility between the dispersed SEBS-*g*-MA and the nylon phase was maximised as revealed by thermal-mechanical analysis. The SEBS was most effective in toughening the nylon/PP blends when it cavitated to introduce ligament bridges between debonded PP particles at the crack tip. Interfacial cavitation and multiple crazing served to relieve the hydrostatic tension ahead of crack growth and subsequently enhanced the shear-yielding component of stresses in the matrix material. Other blend compositions that did not show controlled cavitation resulted in little plastic flow surrounding the crack tip and reduced fracture toughness. These results reinforced the notion that cavitation of SEBS at the nylon–PP interface was an essential mechanism to promote toughening in materials subjected to high crack tip triaxiality.

Keywords: Blends; Nylon 6,6; SEBS

1. Introduction

The use of functionalised copolymers to strengthen the interface between polymeric components wherein strong interactions are lacking, has emerged to be the industrially preferred route in generating useful products from what would otherwise be grossly incompatible blends. The objectives for using functionalised copolymers are two fold: (1) to decrease the interfacial surface tension; and (2) to increase the chain entanglement within the interphase. In Part 1 of this study [1], we attempted to modify the interface between nylon 6,6 and polypropylene (PP) using maleic anhydride (MA)-grafted styrene–ethylene/butylene–styrene (SEBS) copolymers. Fracture toughness was discussed in light of the micro-morphology observed and the tensile deformation of the materials. Success in strengthening the interface between nylon 6 and PP using MA-grafted styrenic block copolymers was reported by Gonzalez-Montiel et al. [2–4]. MA grafted SEBS was found to serve both as a coupling agent and an impact modifier arising from its elastomeric segments. In the blends containing SEBS-*g*-MA, it is understood that the non-polar olefinic rubber can mix well with the PP domains and the grafted anhydride groups exhibit a strong affinity for the amine-end groups on nylons, which subsequently establish an imide linkage with SEBS at the interphase. This combination gives rise to the attractive scenario of using functionalised styrenic block copolymers in strengthening the interfaces of nylon-based blends in the presence of non-polar polymers [2–9]. Nevertheless, the exact nature and the sequence of events that lead to toughening in this ternary system are still unknown. This is particularly true when the triaxial stresses around a sharp crack are taken into consideration. In this paper, we seek to address some of

* Corresponding author. Tel.: +61-2-9351-2290; fax: +61-2-9351-3760.
E-mail address: mai@mech.eng.usyd.edu.au (Y.-W. Mai).
[1] Present address: Division of Materials Engineering, School of Applied Science, Nanyang Technological University, Nanyang Avenue, Singapore 639798.

0032-3861/00/$ - see front matter
PII: S0032-3861(99)00750-8

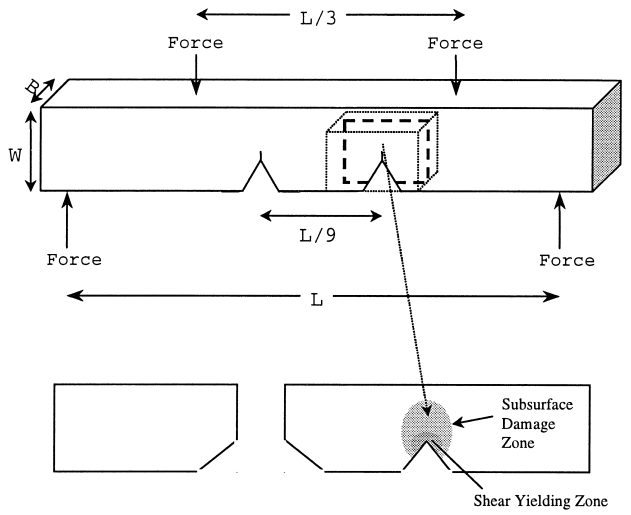

Fig. 1. A schematic of the DN-4PN geometry: ($L = 90$ mm; $W = 12.6$ mm; $B = 5.8$ mm) and the sub-fracture surface damage zone. After Ref. [23]

the potential mechanisms in toughening polymer blends containing functionalised copolymers under triaxial constraint at fracture.

Toughening mechanisms in rubber-modified single-phase polymers have been well established [10–19]. Current understanding associated with matrices that prefer shear yielding to crazing is that internal cavitation of the elastomeric phase can relieve stress triaxiality ahead of flaws, thereby enhancing localised shear deformation [11–16]. Similar mechanisms associated with crazing followed by shear yielding were also reported in PA/PPO [20]. Both cavitation and crazing are dilatational processes, which require sufficient hydrostatic tension for their occurrence. Hydrostatic tension can be optimised by enhancing the geometric constraint such as in single-edge notch-bend (SENB) or single-edge notch-tension (SENT) specimens. Under uniaxial loading, a smooth specimen without a crack is subjected to minimal hydrostatic tension, which only suffices to activate cavitation in materials with low cavitation resistance. Cavitation stress in turn depends on the mechanical property profiles, for example, the bulk modulus of the elastomer versus that of the matrix and their interfacial adhesion [21]. Using three-dimensional finite element analysis, Chen and Mai [21] recently reported the effect of triaxial constraint on the sequence of events that lead to rubber toughening. It was pointed out that rubber inclusions served as stress concentrators like voids only if the effect of triaxial constraint was ignored. Results obtained from uniaxial tensile tests or tensile dilatometry cannot fully reflect the realistic demands in the presence of flaws and thus in engineering applications. Likewise, the understanding involved with global deformation cannot be directly translated into that of the localised situation in the presence of a sharp crack or a notch. It is necessary to study the toughening mechanisms definitively using microscopic techniques in the latter case. In Part II here, we continue to examine the toughening mechanisms in the presence of a sharp crack.

Our work in Part I [1] showed that synergistic toughening indeed occurred when a proper ratio of maleated to non-maleated copolymers was added to the nylon 6,6/PP blends. It was demonstrated that morphological control arising from the copolymer mixtures was determined by the content of MA-grafted SEBS in the system [1]. This is because the anhydride functional group tends to draw grafted SEBS into the nylon matrix from the nylon–PP interface, forming immiscible aggregates in the nylon phase [1]. We concluded that uniformly dispersed SEBS sub-micron particles in the PA matrix coupled with a fine interphase comprising SEBS copolymers around the PP domains would give rise to a morphology that emulates the core-shell rubber modified thermoplastics, as pointed out by Rösch and Mülhaupt [8] and Holsti-Meittinen et al. [7]. The question that remains to be answered in this paper is how exactly this core-shell morphology can effect toughening in SEBS-modified nylon 6,6/PP blends, particularly in the presence of a sharp crack. Conventional wisdom points us to an examination of the interface between nylon 6,6 and PP; the sequence of events that are operative at fracture also plays a critical role in toughening.

Using a petro-thin sectioning technique [22] coupled with transmission optical microscopy (TOM), we compared the deformation zones surrounding the crack tips in the materials studied. Double-notch four-point-bend (DN-4PB) specimen [23] was used to elucidate the sequence of events that operated at fracture. The fracture mechanisms were definitively identified using transmission electron microscopy (TEM) as a function of distance away from the crack tip prepared by the DN-4PB technique. Fractographic examination with scanning electron microscopy (SEM) was employed to consolidate the TEM observations. These results will be discussed with reference to the undeformed microstructures that were reported elsewhere [1].

2. Experimental work

2.1. Materials

The materials investigated were blends of nylon 6,6/PP modified by a mixture of MA grafted and non-grafted SEBS. Materials were dry blended simultaneously at weight ratios of 75/25 PA 66/PP plus 20 wt% SEBS/SEBS-*g*-MA mixture ranging from 0 to 100 wt% SEBS-*g*-MA at five different intervals [1]. It was found that morphological differences arising from the copolymer mixtures were best described in terms of the overall MA content given by MA-grafted SEBS in the mixtures [1], that is, the levels of MA were 0, 0.37, 0.92, 1.47 and 1.84%. In the discussion that follows we shall refer to each blend composition as a given percent-maleated blend independently. Nylon 6,6 resin (Vydyne 21) was supplied by Monsanto Chemical Company

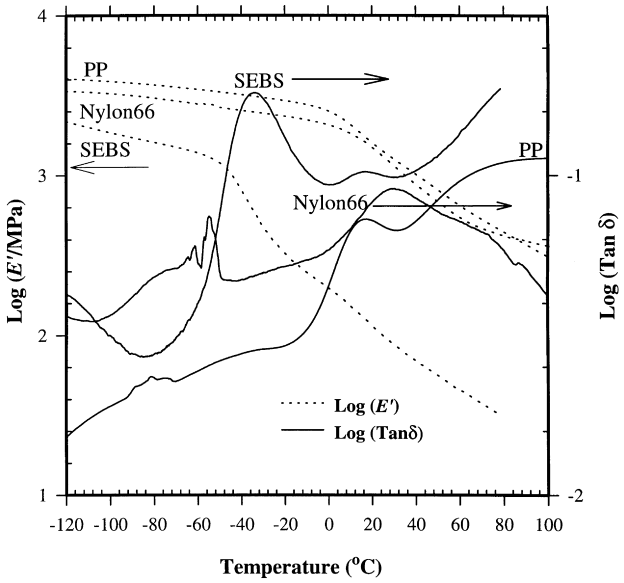

Fig. 2. A composite plot of the storage modulus and loss tan δ of nylon 6,6, PP and SEBS-*g*-MA as a function of temperature.

and PP (Propathene GSE52) was obtained from ICI Australia. The non-maleated triblock copolymer SEBS (Kraton G1652) and its 1.84%-maleated version (Kraton F1901X) were supplied by Shell Chemical. Compounding of the nylon 6,6/PP blends with 20 wt% SEBS/SEBS-*g*-MA was carried out using a twin screw extruder (Werner & Pfleiderer ZSK 30) at a temperature around 270°C, followed by injection moulding (BOY 22S Dipronic). All materials were dried at 60°C in a vacuum oven under reduced pressure prior to compounding and in an oven before being injection moulded into 6 mm thick Izod bars and 3 mm thick dog-bone bars in this study.

2.2. Experimental procedure

TEM analysis was employed to identify fracture mechanisms near the crack tip of 75/25 nylon 6,6/PP. DN-4PB technique was used to disclose the fracture mechanisms under TEM. The technique involves loading a specimen containing two identical cracks in four-point bend geometry as shown in Fig. 1. One of the cracks reached the critical state first and fractured, while a sub-critical damage zone was formed in front of the other initiated but non-propagated crack. A wedge was inserted into the machined notch to sustain the sub-critical crack open while unloading. A specimen block containing this open crack was then cut and embedded in an optically transparent epoxy block, which was cut into a rectangle so that it could fit into the specimen holder for the cryo-microtome. The specimen was ground by ~3 mm exposing the sub-fracture surface on the mid-plane, which was subjected to the highest hydrostatic tension. To study the deformed region using TEM (Philips CM12), the sample surface was further trimmed down to a rectangular surface for cryo-sectioning. Ultra-thin sections were slowly (0.2 mm/s) sliced off at about −40°C from the surface using a diamond knife in a Reichert Ultracut S microtome. The ultra-thin sections were picked up dry as discussed in Ref. [1]. Two staining techniques were used and compared in this work in order to reveal the micro-morphology of the second-phase particles. The first set of sections was stained in 2% aqueous phosphotungstic acid (PTA) mixed with 2% benzyl alcohol for 0.5 h to reveal the nylon phase, leaving the rubber and PP particles unstained unless otherwise specified. The second set of specimens was vapour stained for 0.5 h by RuO_4 prepared in situ. A representative sample of a tensile specimen loaded to fracture of the 0.92%-maleated blend was also studied following the same procedure of embedding, cutting and staining with PTA only so as to compare the plane strain constraint under uniaxial load.

The overall deformation zone as shown in Fig. 1 from the DN-4PB specimen was observed under TOM. The bulk polymer sample containing the damage zone was potted in an optically transparent epoxy block. After being fully cured at ambient temperature one face of the sample was ground and wet polished through several grades of alumina-coated paper and diamond paste-impregnated cloth down to about 2–2.5 mm deep in a 6 mm thick specimen. This polished surface was then glued onto a glass slide using fast cure epoxy resin. The opposite face of the sample was then cut, ground and subsequently polished using a BUEHLER PETRO-THIN sectioning system until it was thin enough to transmit light.

Fractographic examinations of single edge notch bend (SENB) specimens were carried out on gold–palladium coated samples with a Philips 505 SEM. Measurements of dynamic mechanical properties were made using a single cantilever beam fixture under cyclic loading at 1 Hz in a TA Instruments Dynamic Mechanical Analyser 2980 system.

3. Dynamic mechanical analysis (DMA) of phase compatibility

A study of the toughening mechanisms in a complex system consisting of ternary phases must take into account the existing micro-morphology. Having examined the microstructures of nylon 6,6/PP blends containing SEBS-*g*-MA using microscopic techniques [1], we would substantiate our understanding by the dynamic mechanical properties of the studied blends. Thermal-mechanical transitions of multiphase polymers can be readily disclosed using highly sensitive DMA measurements. Fig. 2 is a composite plot of the storage modulus E' and loss tan δ of the component polymers in the selected blends. The storage modulus E' is directly related to the elastic response of the tested materials and tan δ is intimately associated with the chain relaxation that takes place. Note that the glassy transition of SEBS-*g*-MA occurs at −55 to −5°C with a peak at about −30°C. This peak is primarily attributed to the

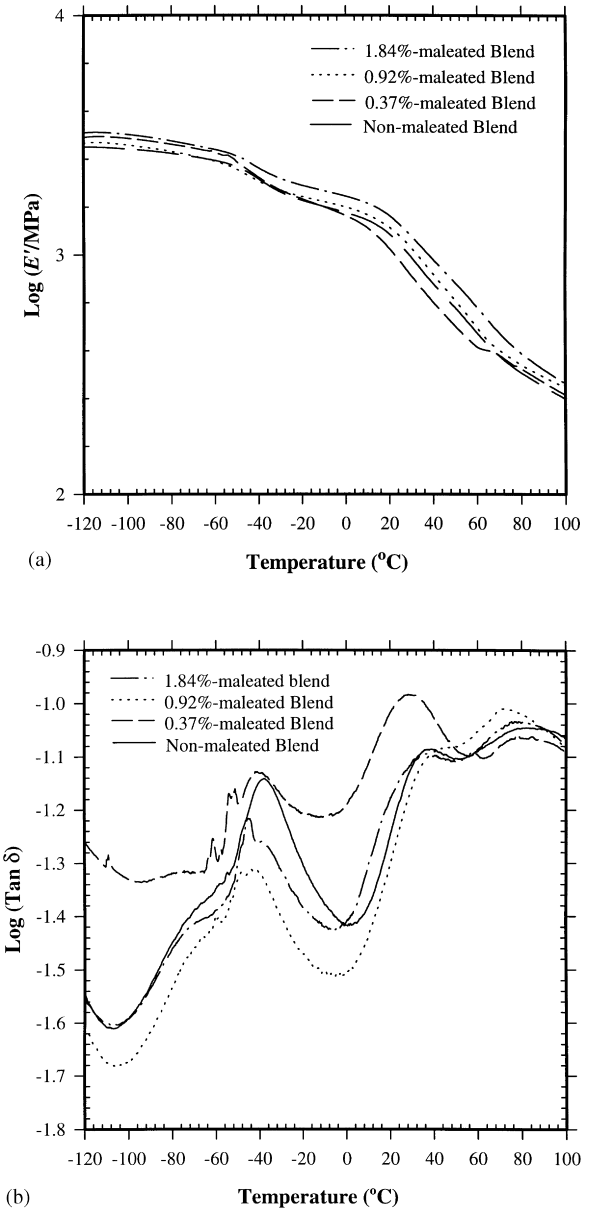

Fig. 3. Composite plots of: (a) the storage modulus; and (b) loss tan δ for selected blends.

rubbery olefinic blocks whereas the rising peak close to 90°C can be attributed to the styrenic blocks, which constitute 26 wt% of the SEBS copolymers [1,2]. The glassy transition peak of nylon 6,6 is noted at around 30°C and there exists a β-transition of PP at −10 to 35°C and a α-relaxation [7] peak around 90°C.

A composite plot of the storage modulus for selected blends is shown in Fig. 3a. All curves experience a gradual decline in E' with increase in temperature from −120 to 100°C, as expected. They show two or more transitions in E' in the heating cycle, which are indicative of immiscibility of the component polymers. A plot of their loss tan δ reveals more clearly the corresponding transition temperatures and the breadth of transition zones (Fig. 3b). The first set of distinct transition peaks arises from the rubbery relaxation near −38°C. The second peaks are primarily associated with the nylon phase and a small proportion of the PP phase (Fig. 2) near 30°C. The third transition peaks are displayed near 80°C, which are attributed to the styrenic blocks in the SEBS and the α-relaxation [7] of the PP phase. The most interesting observation in Fig. 3b is the transitions that take place between 30 and 80°C for the 0.92%-maleated blend showing a tendency to merge together, with one peak forming a shoulder on the other. A broadened transition is noted. However, all other blend compositions show distinctive transitions in this region. This striking result is attributed to the excellent mixing of the MA grafted SEBS in the nylon phase and the well-dispersed PP domains in the matrix. For the 0.37%-maleated blend, where a very thick layer of SEBS-*g*-MA was present at the nylon–PP interface [1], the mixing of the deprived SEBS sub-inclusions in the nylon phase appears to be less efficient than that in 0.92%-maleated system. The PP phase also is not as well dispersed in the nylon matrix as the mixture with one step higher of grafted anhydride content. In the cases with either no anhydride grafted SEBS or the highest level (1.84%) of anhydride grafted SEBS, both show distinct transitions owing to the nylon phase and the SEBS domains, respectively. This understanding is also consistent with the observed rubbery relaxation around −38°C. The 0.92%-maleated blend shows the least transition due to the segregated rubbery sub-inclusions, the result of which is indicative of a comparatively small segregated volume of SEBS available to undergo glassy transition. In contrast, the non-maleated blend shows the most dramatic transition owing to the segregated rubbery phase, which reflects the extraordinarily large phase volume of poorly mixed SEBS that undergoes a glassy transition. For the blend containing the highest level (1.84%) of MA-grafted SEBS, it is clear that the rubbery transition remains remarkable owing to the immiscible aggregates of SEBS in the nylon phase as reported in Part I [1]. Recall that the anhydride functional group tends to draw grafted SEBS into the nylon phase from the PP domains and the nylon–PP interface, forming immiscible aggregates in the nylon matrix. A balance of well-mixed SEBS in the nylon phase and grafted SEBS at the interface was suggested to achieve the best morphology and good PP dispersions.

4. Comparison of crack tip deformation zones using DN-4PB specimens

This paper is focused on understanding the toughening mechanisms of nylon 6,6/PP blends containing SEBS-*g*-MA in the presence of a sharp crack. To gain a general perspective of how the crack tip deformation takes place, we will take a broad view of the deformed zones. Fig. 4 compares the crack tip deformation zones in 0-, 0.37-, 0.92- and 1.84%-maleated SEBS blends under triaxial states of stress.

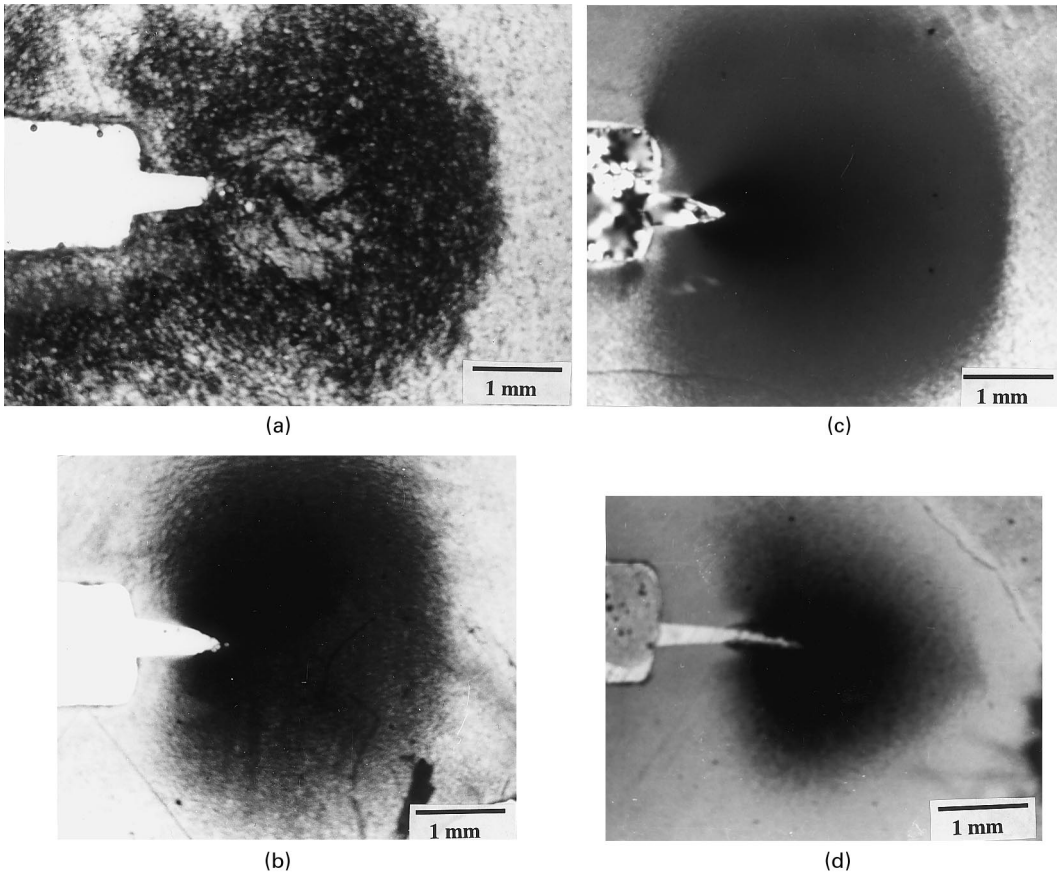

Fig. 4. Crack-tip sub-fracture surface deformation zones for: (a) non-maleated; (b) 0.37-; (c) 0.92-; and (d) 1.84%-maleated blends.

The non-maleated blend (Fig. 4a) shows a very coarse deformation zone when polished to below 100 μm thick. This coarse appearance is consistent with the poor microstructures as revealed under SEM reported in Fig. 2a of our Part I paper [1] and also with the DMA results reported above. Furthermore, the undeformed specimen also gives a cheesy appearance caused by the large interfacial surface tension. Large interfacial cracks prevail in front of the crack tip because of the lack of adhesion between the PP dispersed phase and the nylon 6,6 predominant phase. Addition of 0.37%-maleated SEBS (Fig. 2b) sufficiently enhances the compatibility between the component phases [1] and brings about a much finer deformation zone around the crack tip. Further increase in the grafted MA content refines the phase dispersion and the deformed zone, which shows severe plastic flow around the crack tip (Fig. 4c). However, the crack-tip damage zone for the 1.84%-maleated blend appears markedly diminished (Fig. 4d). This is likely to be caused by the lack of an interphase layer of reasonable thickness as a result of the poor dispersions of the PP domains and the SEBS aggregates [1] in the nylon phase. The major distinction in deformation between the non-maleated blend and over-maleated blend is the occurrence of premature interfacial cracks due to poor compatibility in the former; whereas the latter experiences severe plastic constraint, which is relieved by crack extension and massive cracking at the nylon–PP interfaces. Note that the interfacial adhesion in the 1.84%-maleated blend is still able to sustain post-yield failure [1] primarily due to the "interface" between the highly grafted SEBS on the nylon phase and the PP domains.

5. Microscopic studies of fracture mechanisms

5.1. Studies on the sequence of events at fracture for 0.37- and 0.92%-maleated blends

The power of preserving the deformation history using cryo-ultra-microtomy is excellent. Fig. 5 contrasts the PTA-stained TEM images from an undeformed sample (Fig. 5a), a deformed sample from the crack tip damage zone (Fig. 5b) and a deformed sample under uniaxial loading (Fig. 5c) at the same magnification for the 0.92%-maleated blend. PTA stains the nylon phase dark and gently stains the SEBS at the interphase grey, leaving large PP and small SEBS particles unstained as revealed on the photomicrographs. Clearly, the initially round PP dispersoids, which indicate the comparatively low interfacial tension, are markedly distorted when the specimen is subjected to crack tip deformation. Recall that there is a strong hydrostatic component in this crack tip damage region despite the apparent plastic flow arising from

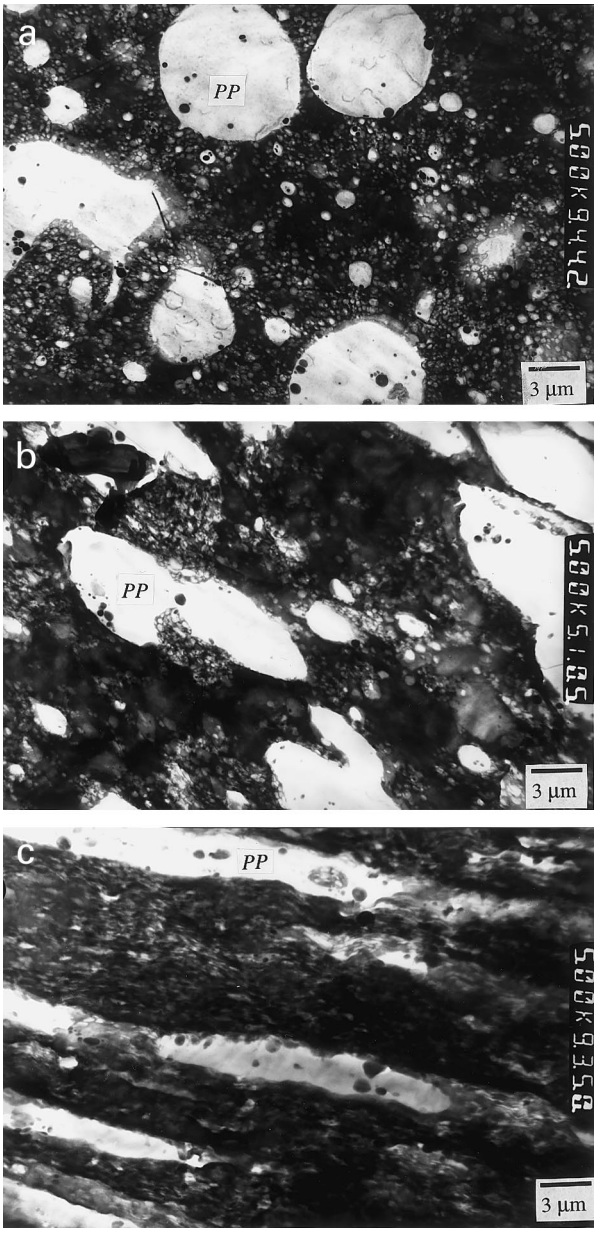

Fig. 5. PTA-stained TEM photomicrographs of 0.92%-maleated blend from: (a) an un-deformed sample; (b) a deformed sample of the crack-tip sub-fracture damage zone from the DN-4PB geometry; and (c) a deformed section of the uniaxially loaded 3 mm thick tensile specimen. Note the dramatic differences in the degree of distortion (deformation) in the PP domains.

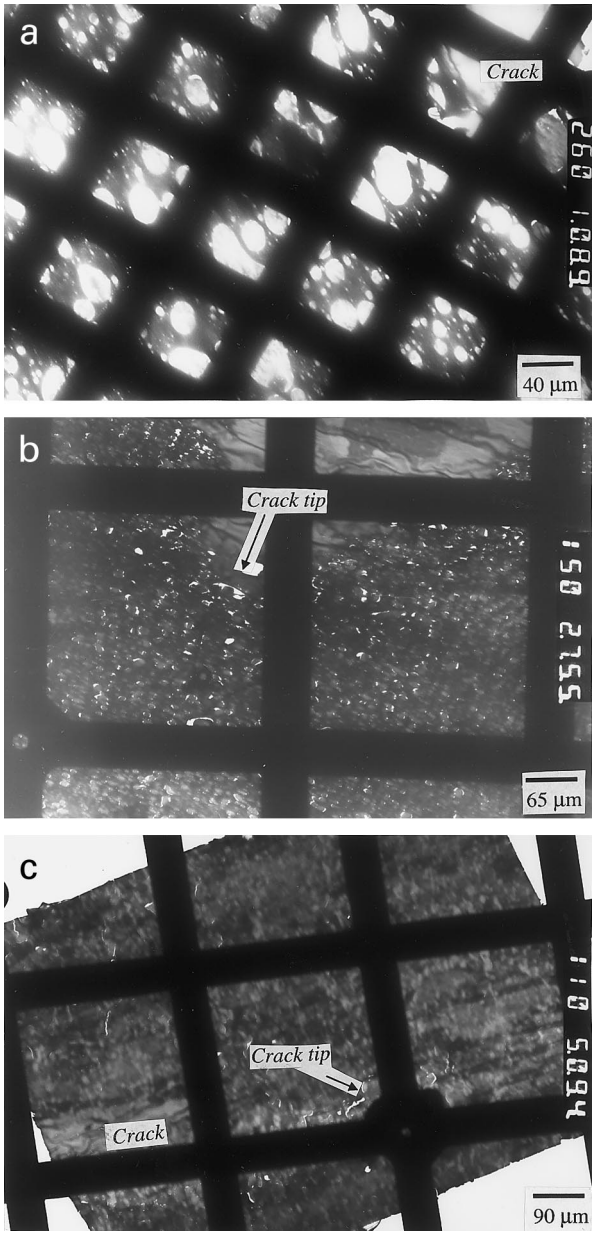

Fig. 6. Representative ultra-thin sections for: (a) 0.37-; (b) 0.92-; and (c) 1.84%-maleated blends. Note that the cracks are sustained open by embedded epoxy.

distortional plasticity. This understanding is important to our subsequent discussion concerning the sequence of events that occur at fracture for the 0.92%-maleated blend. Deformation with little hydrostatic tension can be achieved using a 3 mm thick uniaxially loaded tensile specimen (Fig. 5c). In this case, distortional plasticity prevails and the PP and SEBS domains are elongated by a few hundred percent, which far exceeds what can be generated using DN-4PB specimen. This result not only shows that the deformation behaviour of nylon 6,6/PP blends containing SEBS-*g*-MA is sensitive to crack tip triaxiality, but it also confirms that information obtained from deformation that takes place under simple tension, like tensile dilatometry, cannot represent the true toughening process under triaxial loading. From a mechanics viewpoint, Chen and Mai [21] showed that shear yielding occurred much more readily without transverse constraints, resembling the case wherein the matrix is under simple tension. Under triaxial constraints, the Von-Mises plastic flow stress was increased by 35% in a rubber/epoxy system. And, the effective plastic strain could attain 97% in a void/epoxy system (without transverse constraints) versus 33% in a particle/epoxy system (with triaxiality) adjacent to a crack tip. Similar

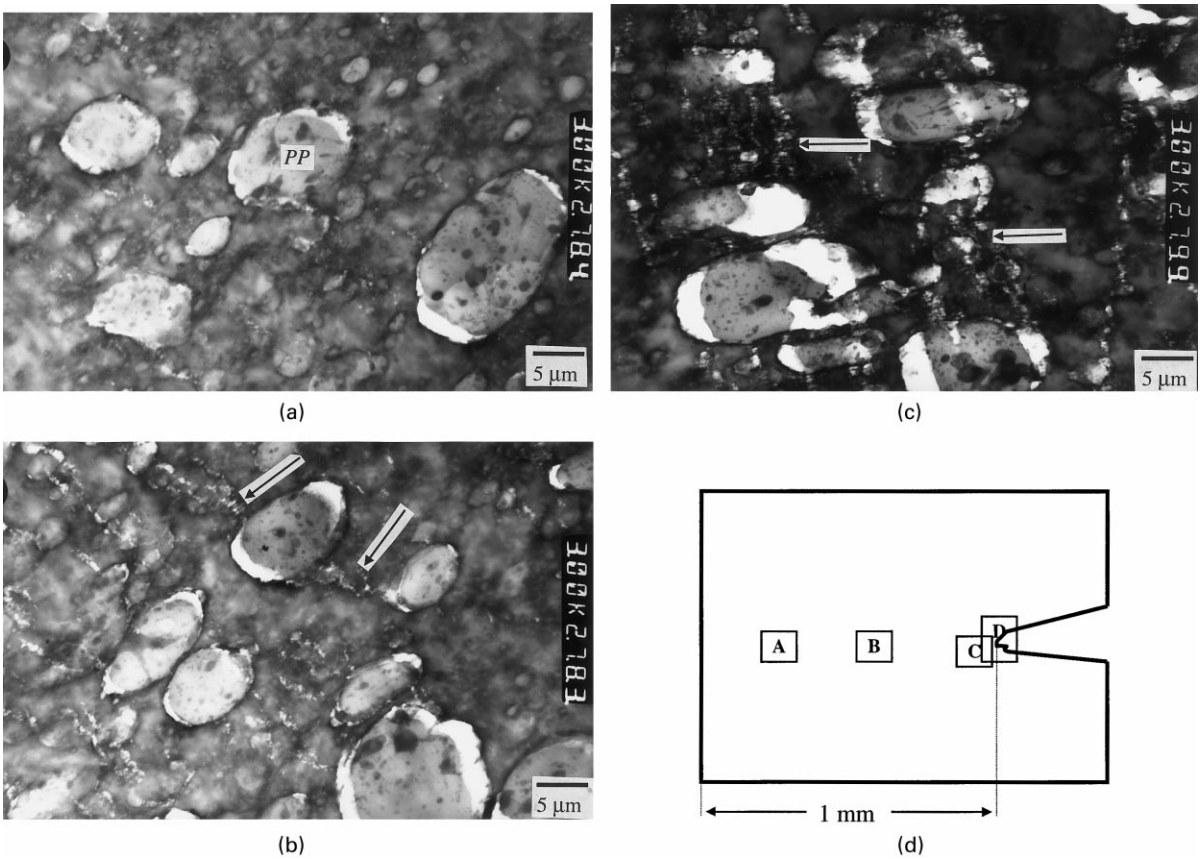

Fig. 7. RuO_4-stained TEM photomicrographs taken as a function of distance away from the crack tip in the 0.92%-maleated blend. (a) Location A, where PP dispersoids appear to be relatively round and cavitation at the interface has occurred. (b) Location B, where crazes emanate from the equators of the debonded PP particles and more severe distortion in the surrounding matrix is noted. (c) Location C, where massive shear deformation can be seen. Locations A, B and C are taken inside the stress-whitened region as indicated in (d). Arrows show the craze structures in (b) and (c).

calculations were reported by Dijkstra and Ten Bolscher [24] on nylon/rubber blends and Chen and Mai [25] on rubber modified PC and PEI/PC blends.

Fig. 6 presents a series of representative ultra-thin sections ready for viewing under TEM. For the 0.37%-maleated blend (Fig. 6a), comparatively large and round PP inclusions can be seen on the copper grid. Immediately adjacent to the crack tip, the PP particles appear somewhat elongated and debonded from the nylon matrix. Farther away from the crack tip, the PP particles appear in fact intact and firmly embedded in the nylon phase with negligible cavitation at the interface. An ultra-thin section from the 0.92%-maleated blend shows a dramatically different picture (Fig. 6b). The crack tip opening was sustained by an epoxy embedded wedge during the embedding process prior to ultra-microtomy. Note that the crack tip has undergone a blunting process at the onset of crack growth. Many small voids near the crack tip region on the ultra-thin sections can be identified under bright field image. These voids in fact arise from the severe plastic flow and PP–nylon interface debonding as we can observe under a higher magnification. The PP domains in the 0.92%-maleated system appear much finer and smaller compared to those in the 0.37% blend. We believe the particle size distributions could alter the stress interactions near the crack tip. A quantitative mechanics model for a ternary-phase rubber-containing system is not available at the present time.

The RuO_4-stained photomicrographs taken as a function of distance away from the crack tip for the 0.92%-maleated blend are shown in Fig. 7. Their respective positions are indicated in Fig. 7d. Fig. 8 shows the PTA-stained photomicrographs that mirror the images in Fig. 7 except for Fig. 8d, which is directly taken at the crack tip. Fig. 7a is the photomicrograph taken at the farthest distance away from the crack tip but within the deformed region. Photomicrograph of an undeformed section was already displayed in Fig. 5a. For the RuO_4-stained sections, the PP dispersoids are stained light grey and the nylon phase is stained dark grey. SEBS is stained dark by RuO_4. Its clear cavities are located at the PP–nylon interfaces. These cavities evidently are internally activated and are debonded SEBS interphase, the process of which relieves the severe hydrostatic tension surrounding the crack tip and enhances localised shear yielding of the SEBS-modified nylon matrix. In this position the surrounding matrix has not fully distorted the PP dispersoids, which have not completely withdrawn from the interface, implying relatively constrained shear flow.

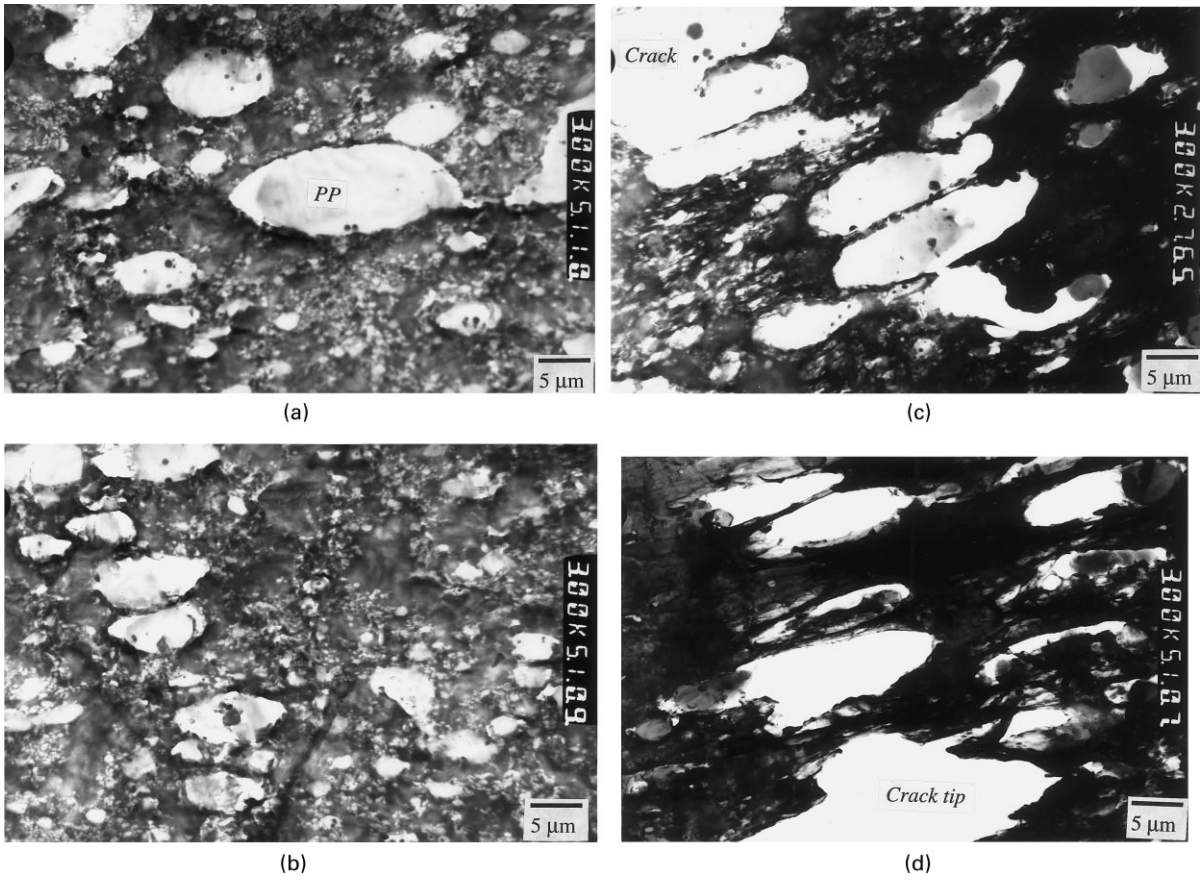

Fig. 8. PTA-stained TEM photomicrographs taken as a function of distance away from the crack tip in the 0.92%-maleated blend. (a) Location A, (b) location B, (c) location C and (d) location D in the stress whitened region as indicated in Fig. 7d.

Moving closer to the crack tip (Fig. 7b), we can observe more extensive interfacial cavitation and debonding of the rubbery phase with some craze-like microvoids (crazes) emanating from the interface and running perpendicular to the elongated direction of the PP dispersoids. We believe that the holes containing debonded SEBS and PP inclusions act as stress concentrators, which nucleate the crazes in the matrix. We also surmise that the crazes are formed by micro-necking and cavitation of the SEBS sub-inclusions in the nylon phase. These crazes have numerous microvoids and a fibrillar microstructure (Fig. 9), which resemble those reported by Friedrich [26] in rubber-modified PETP. Both cavitation and multiple crazing are dilatational processes that absorb a large amount of energy before massive yielding takes place. Their prevalent presence also explains the large stress-whitened zone surrounding the crack tip (Fig. 4c) for the 0.92%-maleated blend. Clearly, the crack tip triaxial stresses promote the dilatational deformation, namely, cavitation followed by multiple crazing. Following the plane strain relief as activated by the dilatational deformation, distortional plasticity is significantly enhanced in the region adjacent to the crack tip (Figs. 7c and 8c). The matrix material is now extensively distorted with PP inclusions withdrawn from the interface. A photomicrograph taken at the crack tip (Fig. 8d) shows the elongated voids formed by the PP inclusions completely detached from the interface on the ultra-thin section. The crack faces are sustained by the SEBS–nylon bridges, which have undergone significant yielding prior to fracture. This massive matrix yielding plays the predominant role in enhancing the *J*-integral fracture toughness for the SENB specimen.

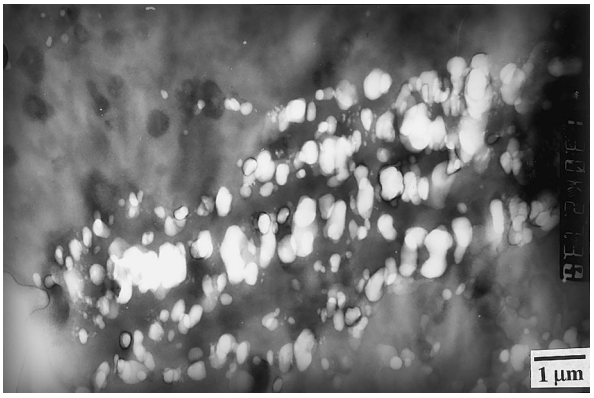

Fig. 9. Enlarged image of the craze microstructures with voids and fibrils found in Fig. 7b and c. The voids are formed by a necking process of the matrix ligaments and consisted of cavitated SEBS sub-inclusions.

The toughening mechanisms as evidenced in the 0.92%-maleated blend can be summarised as follows. The

Fig. 10. A representative overview of the fracture surface of 75/25 nylon 6,6/PP blends containing SEBS-*g*-MA, showing a markedly curved crack front caused by severe plane stress to plane strain transition across the thickness from the skin to the mid-plane.

sequence of events clearly begins with rubber cavitation and debonding followed by multiple crazing, both of which relieve the hydrostatic component of stresses and subsequently facilitate the volume-conserving yielding mechanism to take place in the remaining matrix component, with nylon ligaments bridging the crack faces prior to crack growth. The SEBS was most effective in toughening the nylon/PP blends when it cavitated to introduce ligament bridges between debonded PP particles at the crack tip. This mechanism was primarily responsible for the extraordinarily high *J*-integral fracture toughness at 0.2 mm crack extension [1]. The importance of cavitation and multiple crazing is dependent on the necessity for constraint relief in promoting shear yielding in the continuous phase [13,27]. With a 3 mm thick tensile specimen under uniaxial load, we reported [1] that debonding of PP domains in the presence of MA-grafted SEBS occurred after the PP phase had been drawn to a significant extent by the nylon matrix. Fig. 5c also illustrates how much greater the elongation of the PP domains together with the surrounding matrix component can happen in the absence of crack tip constraints. Interfacial debonding is not clear along the lateral interface of the highly drawn PP domains in Fig. 5c, which indicates a high Von-Mises stress and a sufficiently strong interphase for post-yield deformation. Cruz and Havriliak [28,29] also reported similar mechanisms involving shear yielding prior to debonding in rubber-modified nylon 6 and PBT, respectively. They observed that the rubber particles were elongated to a large extent before cavitation could occur. Their results are consistent with what we have observed in the uniaxially loaded 3 mm thick specimen. For the 6 mm thick SENB specimen, we observed a severe plane stress–plane strain transition from the skin to the mid-plane of the cross-section on the fracture surface. Fig. 10 is a representative fractograph showing a characteristic crack front in a SENB specimen of 75/25 nylon 6,6/PP blend containing SEBS-*g*-MA. Note the curved crack front generated by severe triaxial stresses near the mid-plane and by the virtually plane stress deformation near the skin. Evidently, the toughening mechanisms under plane stress are different from those under plane strain for the selected material. The essential difference in the sequence of events of whether cavitation-debonding precedes shear flow or vice versa lies in the state of stress concerned. Cavitation ahead of shear yielding is only required under severe plane strain condition [27]. The toughening criteria of one test cannot be directly translated to those obtained from another. A sufficiently strong interphase is, nevertheless, necessary under all circumstances to effect post-yield toughening [12]. In this particular case with 0.92%-maleated system, we believe the relatively fine dispersions of PP surrounded by the SEBS interphase also provide effective stress interactions in enhancing shear deformation after the hydrostatic stress is relieved by cavitation.

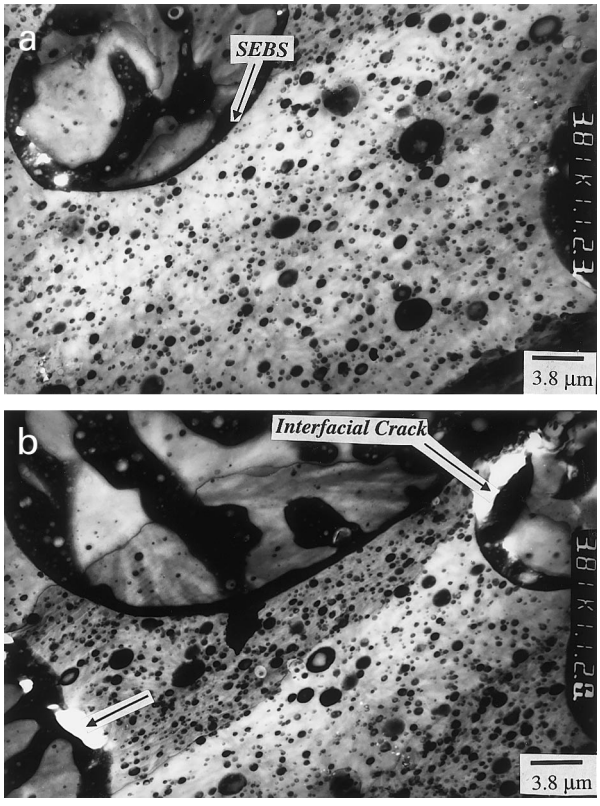

Fig. 11. RuO_4-stained TEM photomicrographs taken as a function of distance away from the crack tip in the 0.37%-maleated blend. (a) Location A and (b) location C in the stress-whitened region as indicated in Fig. 7d. Inside the stress-whitened region near the crack tip, little distortional plasticity is noted. PP domains remain firmly adhered to the matrix by the thick layer of SEBS interphase. No internal cavitation occurred prior to massive interfacial crack near the crack tip.

An interesting observation arises when photomicrographs are taken for the 0.37%-maleated blend (Figs. 11 and 12) in similar locations. The interesting difference is that SEBS cavitation is not seen in this blend composition until near the crack tip, where plastic flow is dramatically constrained. Two representative photomicrographs stained by RuO_4 (Fig.

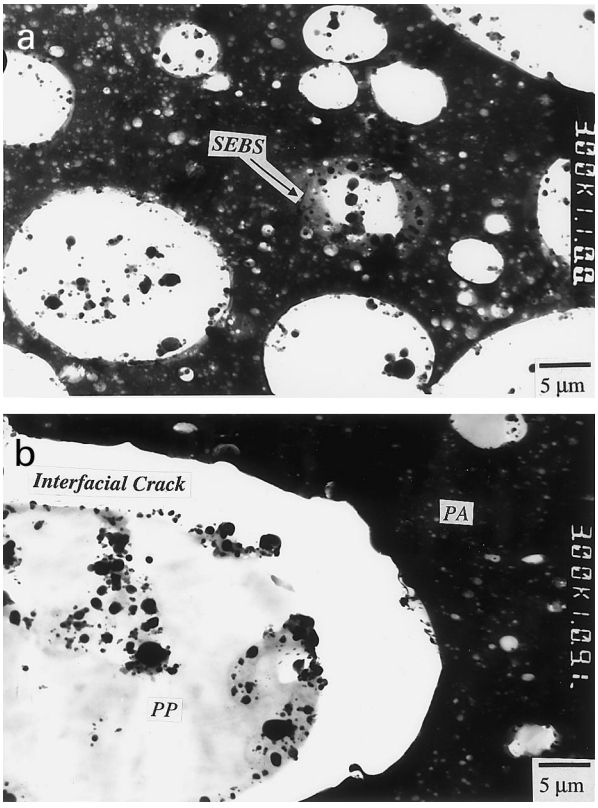

Fig. 12. PTA-stained TEM photomicrographs taken as a function of distance away from the crack tip in the 0.37%-maleated blend. (a) Location A and (b) location C in the stress-whitened region as indicated in Fig. 7d.

11a) and PTA (Fig. 12a), respectively, in location A (Fig. 7d) are chosen to illustrate this point. Although it is well within the crack tip damage zone, the interphase formed by SEBS-*g*-MA, stained dark by RuO_4, appears very thick and the PP inclusions are firmly embedded in the nylon matrix. Moving closer to the crack tip minimal interface debonding is found (Fig. 6a). Only at incipient fracture (location C in Fig. 7d) are large PP domains entirely detached from the rubber-modified nylon matrix (Fig. 12b). Far less plastic flow and little matrix distortion are evident near the crack tip for the 0.37%-maleated blend.

The difference in toughening behaviour between the 0.37- and 0.92%-maleated blends is also evident in the SEM fractographs. Fig. 13 compares the cryo-fractured zones in front of the crack growth region (see Fig. 13e). Cavities are prevalent in the cryo-fractured zone due to the cavitation-debonding mechanism in the 0.92%-maleated blend (Fig. 13a) whereas the PP domains are firmly embedded in the nylon phase in the 0.37%-maleated blend (Fig. 13b). Thick SEBS interphase can be identified in Fig. 13b after impact fracture. Note that the interphase appears intact with minimal degree of cavitation and debonding. Closer to the slow crack growth region, the SEM photomicrographs we reported in our Part I paper [1, Fig. 2b and c] reveal different micro-deformation experienced by the 0.37- and 0.92%-maleated blends. For easy reference, these photomicrographs are reproduced in Fig. 13c and d. Clearly, as shown in Fig. 13c for the 0.92%-maleated blend, partially drawn PP particles protrude from their respective matrix voids, which have also undergone severe plastic tearing and yielding, consistent with TEM photomicrographs shown in Figs. 7c, 8c and d. Conversely, for the 0.37%-maleated blend, the surface of the PP protrusions appears very rough (Fig. 13d), which indicates minimal cavitation prior to breaking apart from the nylon matrix. The debonded cavities at the onset of crack growth are consistent with those shown in a thin-sectioned sample on TEM photomicrograph (Fig. 12b). The deformation behaviours as seen in these SEM fractographs strongly support TEM observations we made in Figs. 6–9, 11 and 12. That is, cavitation and debonding at the interphase are suppressed in the 0.37%-maleated blend; the hydrostatic tension around the crack tip remains high and plastic flow in the matrix is markedly constrained, leading to a low *J*-integral fracture toughness in comparison to the 0.92%-maleated blend [1]. Our results, however, do not confirm that thick interphase layer prohibits rubber cavitation and debonding. For rubber-toughened single-phase polymers, it is understood that the rubbery phase is perfectly capable of cavitating or debonding on reaching a critical stress but crack extension or particle size could limit the volume of material within which stresses reach a sufficient level to cause cavitation and subsequent shear yielding. Nevertheless, rubber particle size [30] also plays a pivotal role in activating the toughening mechanisms in binary phase polymers. In the materials studied, PP domain size varied from relatively large particles in 0.37% to relatively small particles in 0.92% followed by larger particles in blends containing higher MA content. At 0.37% MA, we conjecture that the balance between cavitation/yielding, particle size and crack growth is less favourable than that at 0.92% MA. Furthermore, it is believed [31] that in our three-phase system, as the thickness of SEBS increases, the stresses acting at the interphases will change. The stresses that can be transmitted to the interphase boundary of the SEBS-PP particle will be decreased because the elastic modulus of SEBS is smaller than nylon and PP. This will *reduce* the capability of interphase debonding. However, it is not immediately clear how the stresses in the SEBS layer will be altered. We cannot therefore predict a priori if a thicker SEBS layer will decrease the stresses (suppressing cavitation) or vice versa (favouring cavitation). More analytical and numerical modelling work is necessary to provide further insight into this problem.

5.2. 1.84%-maleated blend

The ultra-thin section of the 1.84%-maleated blend was shown in Fig. 6c. The partially propagated crack was kept open with an epoxy embedded wedge. The whole section surrounding the crack tip appears very well preserved with some large interfacial fissures sparingly identified at the crack tip. Detailed examination of the photomicrographs

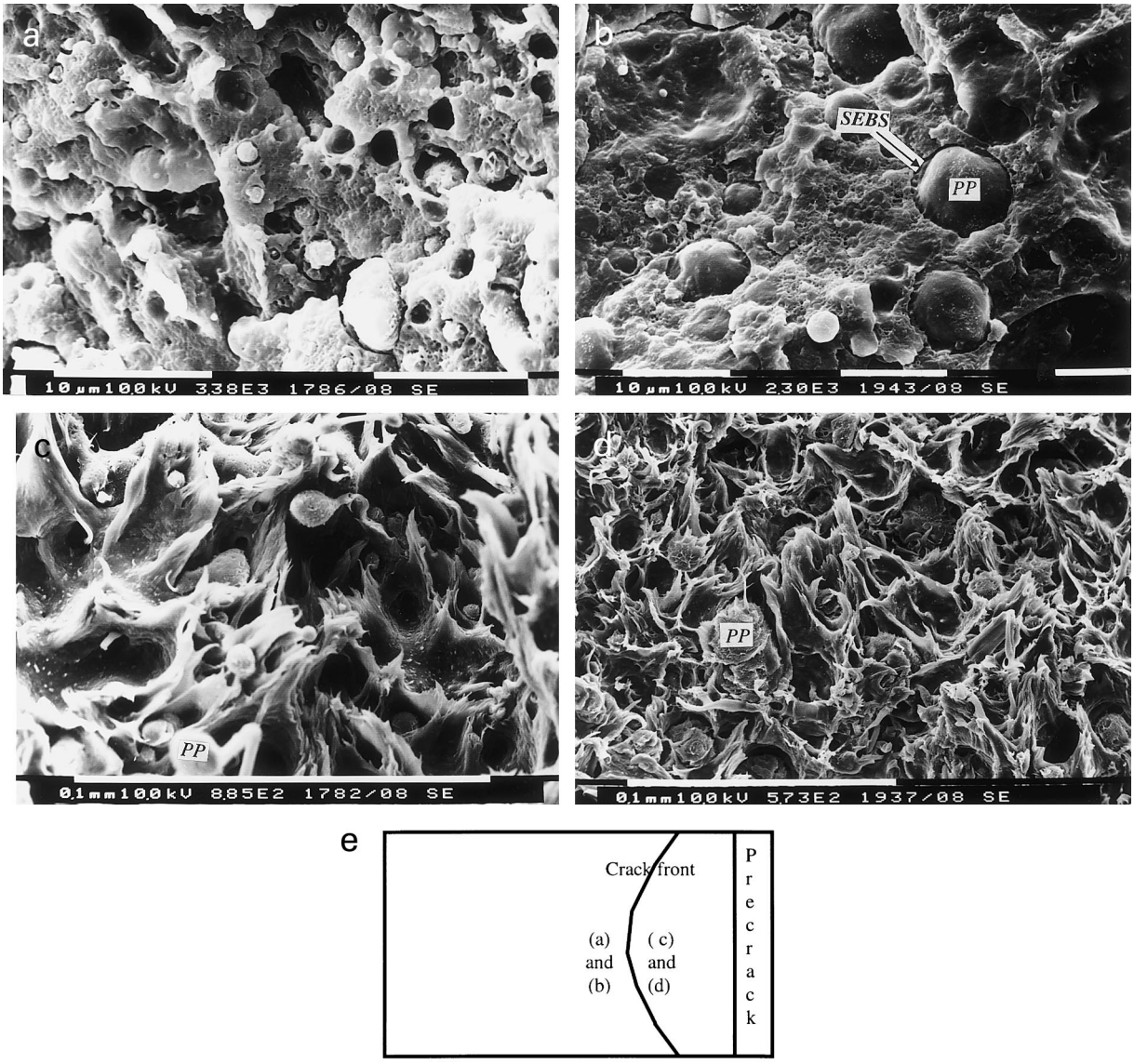

Fig. 13. SEM fractographs showing the cryo-fractured zones in: (a) 0.92%-maleated blend, where cavitation is noted ahead of crack growth; and (b) 0.37%-maleated blend, where PP domains remain firmly adhered to the matrix by the thick layer of SEBS interphase. SEM fractographs in the crack growth regions are shown in: (c) for 0.92%-maleated blend; and (d) for 0.37%-maleated blend. Respective locations of (a), (b), (c) and (d) taken from the fracture surface are displayed in (e).

(Fig. 14) as a function of distance away from the crack tip shows little plastic flow before fracture. The dispersion of PP domains is extremely poor and the MA-grafted SEBS forms aggregates as revealed by the sub-inclusions in the nylon phase (Fig. 14a and b). The poor dispersion of the PP domains is also evident on the cryo-fractured surface in front of the crack growth region under the SEM (Fig. 4 in Part I). We believe, however, that the interfacial adhesion remains considerably strong, which is supported by the comparatively high tensile strength reported earlier [1]. But the lack of interfacial cavitation caused by the poor PP dispersion contributes to the high triaxial constraint prior to crack growth. Consequently, the matrix material is unable to yield before fracture, consistent with the small plastic damage as revealed in the optical photomicrographs. Little energy is dissipated before large interfacial cracks are formed (Fig. 14c) at failure and a reduced fracture toughness ensued [1]. Fig. 15 summarises the sequence of events at fracture for the 0.37-, 0.92- and 1.84%-maleated blends.

6. Conclusions

The interfacial behaviour of the component phases was studied under cyclic fatigue loading in a dynamic mechanical analyser as a function of temperature. It was found that for the 0.92%-maleated blend, nylon 6,6 and SEBS exhibited optimal miscibility, which supported the

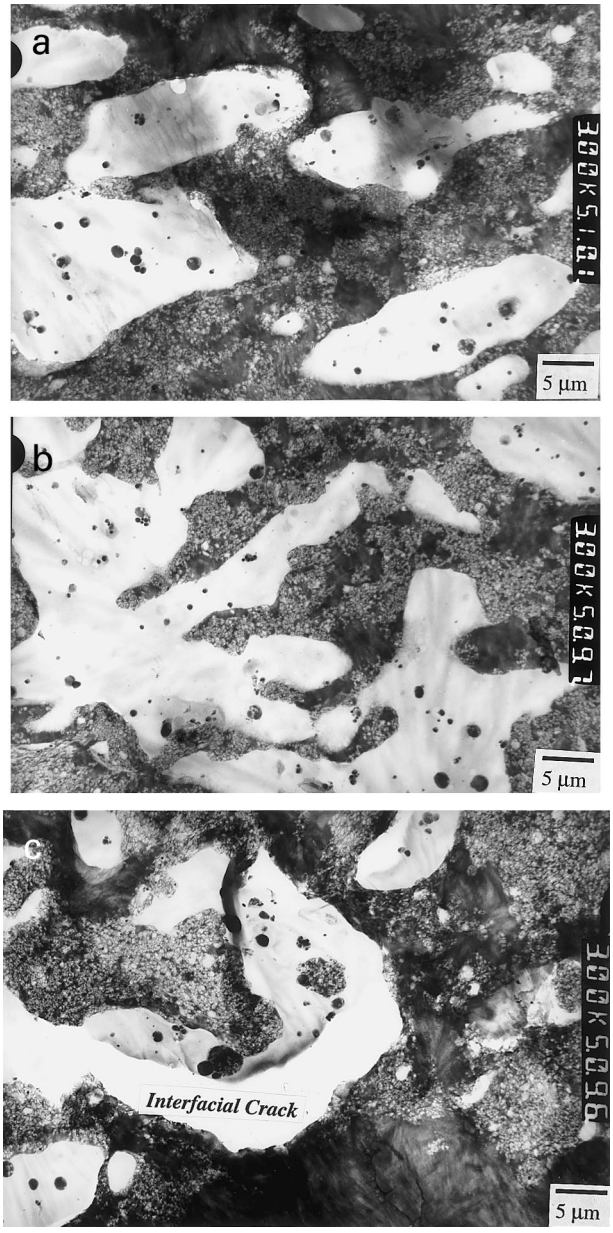

Fig. 14. PTA-stained TEM photomicrographs taken as a function of distance away from the crack tip in the 1.84%-maleated blend. (a) Location A, (b) location B and (c) location C in the stress-whitened region as indicated in Fig. 7d.

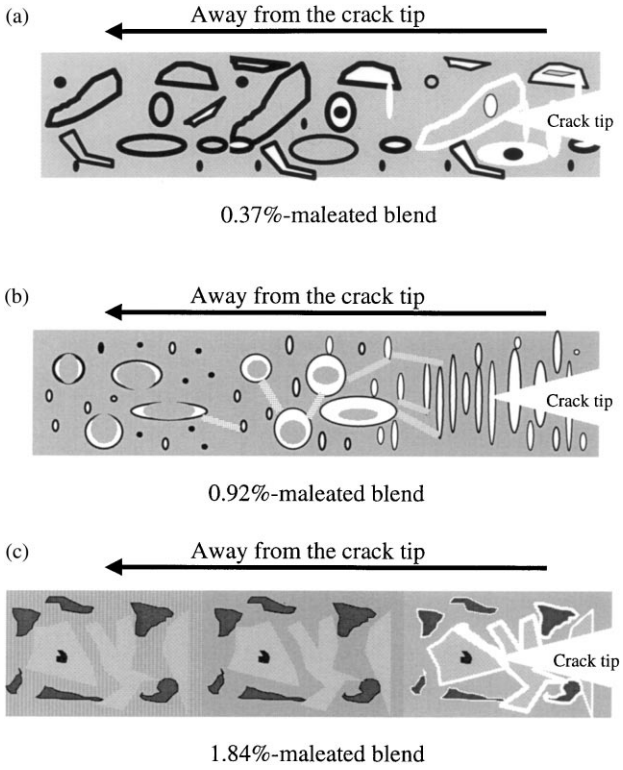

Fig. 15. Schematic of the sequence of fracture events in: (a) 0.37%-; (b) 0.92%-; and (c) 1.84%-maleated blends.

comparatively good morphology noted elsewhere [1]. Also, the PP domains were well dispersed in the 0.92%-grafted MA mixture, a direct result of lower interfacial tension due to enhanced miscibility at the interface.

The sequence of events in deformation of the nylon 6,6/PP blends containing SEBS-*g*-MA was convincingly demonstrated by microscopic techniques. To achieve effective toughening, we showed that the state of stress was critical to the toughening mechanisms involved with the same materials. Under triaxial stress, it was shown that cavitation of the SEBS-*g*-MA interphase occurred prior to multiple crazing in the SEBS-modified nylon, which was followed by massive shear yielding at the crack tip. The cavitation and crazing served to relieve the triaxial constraint and subsequently activated the distortional plasticity in the matrix ligaments. Internal cavitation and/or debonding of SEBS-*g*-MA were not observed in 0.37%-maleated bend, where extraordinarily large PP particles are surrounded by thick layers of SEBS, leading to an inability to relieve plane strain constraint and subsequently unable to promote shear flow in the matrix. The fracture toughness in this case would be considerably reduced. High surface tension contributed to poor dispersions of the PP domains in the blends containing high MA content, which also inhibited internal cavitation and led to large interfacial cracks at fracture. The major energy dissipation mechanism still relied on the plastic flow of the matrix, without which all materials showed diminished fracture toughness in contrast to the comparatively higher tensile strength or stiffness.

Acknowledgements

The authors would like to thank the Australian Research Council (ARC) for the continuing support of this polymer blends project. S.-C. Wong acknowledges the award of a Postgraduate Research Scholarship funded by the ARC and tenable at the University of Sydney. Monsanto Company

supplied the nylon 6,6 resins; Shell Chemical provided the impact modifiers and ICI Australia the PP resins. Thanks are due to the Electron Microscope Unit at the University of Sydney for providing access to its characterisation facilities. A note of deep appreciation is extended to the referee who has made so many brainstorming remarks and constructive comments that ultimately improve the quality of the final paper.

References

[1] Wong S-C, Mai Y-W. Polymer 1999;40:1553.
[2] Gonzalez-Montiel A, Keskkula H, Paul DR. Polymer 1995;36:4587.
[3] Gonzalez-Montiel A, Keskkula H, Paul DR. Polymer 1995;36:4605.
[4] Gonzalez-Montiel A, Keskkula H, Paul DR. Polymer 1995;36:4621.
[5] Gelles R, Modic M, Kirkpatrick J. Modification of engineering thermoplastics with functionalized styrenic block copolymers. In: Proceedings of the Society of the Plastic Engineering 46th Annual Technical Conference, ANTEC 1988, p. 513.
[6] Modic MJ. Compatibilization of Polyamide/polyolefin blends with functionalized styrenic block copolymers. In: Proceedings of the Society of the Plastic Engineering 51st Annual Technical Conference, ANTEC 1993, p. 205.
[7] Holsti-Miettinen RM, Seppälä JV, Ikkala OT, Reima IT. Polym Engng Sci 1993;34:395.
[8] Rösch J, Mülhaupt R. Polym Bull 1994;32:697.
[9] Rösch J. Polym Eng Sci 1995;35:1917.
[10] Bucknall CB. Toughened plastics, London: Applied Science, 1977.
[11] Bucknall CB, Heather P, Lazzeri A. J Mater Sci 1989;24:1489.
[12] Bucknall CB, Soares VLP, Lazzeri A. In: Choy CL, Shin FG, editors. Proceedings of the International Symposium on Polymer Alloys and Composites, Hong Kong: Hong Kong Polytechnic University, 1992. p. 104–20.
[13] Yee AF, Li D, Li X. J Mater Sci 1993;28:6392.
[14] Parker DS, Sue H-J, Huang J, Yee AF. Polymer 1990;31:2267.
[15] Pearson RA, Yee AF. J Mater Sci 1986;21:2475.
[16] Donald AM, Kramer EJ. J Mater Sci 1982;17:1765.
[17] Kinloch AJ, Shaw SJ, Hunston DL. Polymer 1983;24:1355.
[18] Kinloch AJ, Shaw SJ, Tod DA, Hunston DL. Polymer 1983;24:1341.
[19] Kinloch AJ. In: Riew KC, editor. Rubber-toughened plastics, Advances in Chemistry Series, 222. Washington, DC: American Chemical Society, 1989. p. 67–91.
[20] Sue H-J, Yee AF. J Mater Sci 1989;24:1447.
[21] Chen XH, Mai Y-W. Key Eng Mater 1998;137:115.
[22] Takemori MT, Yee AF. Impact fracture of polymers—materials science and testing techniques. In: Takahashi K, Yee AF, editors. Fukuoka-shi, Japan: Kyushu University, 1992. p. 331–92.
[23] Sue H-J, Yee AF. J Mater Sci 1993;28:2975.
[24] Dijkstra K, Ten Bolscher GH. J Mater Sci 1994;29:4286.
[25] Chen XH, Mai Y-W. Three-dimensional elastoplastic finite element modelling of deformation and fracture behaviour for rubber-modified PC at different stress triaxiality. Proceedings of the First Asian-Australiasian Conference on Composite Materials, 7–9 October, Osaka, Japan, 2. 1998. p. 704(1)–4).
[26] Friedrich K. In: Kausch HH, editor. Crazing in polymers, Advances in Polymer Science 52/53, 1. Berlin: Springer, 1983. p. 255.
[27] Yee AF. J Mater Sci 1977;12:757.
[28] Cruz CA Jr., Havriliak S Jr. Role of cavitation in the impact modification of nylon 6. In: Proceedings of the Society of the Plastic Engineering, 53rd Annual Technical Conference, ANTEC 1995, p. 1521–1525.
[29] Cruz Jr. CA, Havriliak Jr. SJ. Impact behavior and high speed tensile testing in toughened poly(butylene terephthalate). Presented in the Society of the Plastic Engineering 56th Annual Technical Conference, ANTEC 1998.
[30] Borggreve RJM, Gaymans RJ, Schuijer J, Ingen Housz JF. Polymer 1987;28:1489.
[31] Wang X. Private communication.